IEEE Access
Multidisciplinary ⋮ Rapid Review ⋮ Open Access Journal

Received 17 October 2023, accepted 4 November 2023, date of publication 8 November 2023,
date of current version 16 November 2023.

Digital Object Identifier 10.1109/ACCESS.2023.3331012

RESEARCH ARTICLE

Vision-Based In-Hand Manipulation for Variously Shaped and Sized Objects by a Robotic Gripper With Active Surfaces

YUZUKA ISOBE[1], SUNHWI KANG[2], TAKESHI SHIMAMOTO[2], YOSHINARI MATSUYAMA[2], SARTHAK PATHAK[3], (Member, IEEE), AND KAZUNORI UMEDA[3], (Member, IEEE)

[1]Graduate School of Science and Engineering, Chuo University, Bunkyo, Tokyo 112-8551, Japan
[2]Research and Development Revision, Panasonic Connect Company Ltd., Chuo, Osaka 540-8553, Japan
[3]Faculty of Science and Engineering, Chuo University, Bunkyo, Tokyo 112-8551, Japan

Corresponding author: Yuzuka Isobe (isobe@sensor.mech.chuo-u.ac.jp)

This work was supported by the New Energy and Industrial Technology Development Organization (NEDO) under Grant JPNP20016.

ABSTRACT In-hand manipulation to translate and rotate an object is a challenging problem for robotic hands. As one solution, robotic hand with belts around fingers (*active surfaces*) has been developed for continuous and seamless manipulation. However, in practice, the grasped object can only be rotated through a small range less than 90° except the objects with simple shapes like cubes and cylinders. This is because the fingers cannot follow the width required not to drop the object or the desired rotation cannot be produced depending on its shape, leading to dropping the object or unable to rotate it anymore. This paper presents a method to address these problems and rotate objects of various shape and sizes through a large range of motion. A stereo camera is attached to a two-fingered robotic hand with belts. The changes in the contact points between the surfaces of the belts and object are predicted. Based on the prediction, the belts are controlled to adjust the angular velocity of the object such that the fingers can follow the width required to grasp it and the appropriate rotation can be produced. The fingers are controlled to follow the predicted contact points and deflect the belts to both cancel the unwanted rotation and generate the desired rotation. Through experiments in which 32 objects of 16 shapes and 2 sizes, and other real-world objects were rotated to 1 revolution, the rotational ranges for various objects were larger than in the other studies, confirming the validity of the proposed method.

INDEX TERMS In-hand manipulation, robotic hand, robot vision, visual servo, active surfaces, belts, gripper, stereo camera, variously shaped, sized objects.

I. INTRODUCTION

In-hand manipulation (IHM) is a challenging problem for robotic hands. Changing the position and orientation of a grasped object without dropping it from the hand workspace is a dexterous task [1], [2], [3], [4]. This task is important for pick-and-place motion, which is a basic ability for robotic hands to be used in various industries, such as manufacturing, logistics, and retail. To realize this task, a robotic hand should be able to both grasp and manipulate the object [4]. That is, the capabilities of maintaining the grasp throughout the processes and manipulating the object to an arbitrary position and orientation are required simultaneously. The grasping capability should show robustness to the variety of the object characteristics (size, shape, orientation, and so on) and the possible disturbances (e.g., unexpected forces or erroneous estimates of the object characteristics) without damaging the object [3]. The manipulation capability should show the range of manipulation (translation and rotation of the objects), i.e., how large a range of translational displacement and rotational angle can be achieved. Manipulating various types of objects through a large range of motion (especially rotation) within

The associate editor coordinating the review of this manuscript and approving it for publication was Thomas Canhao Xu.

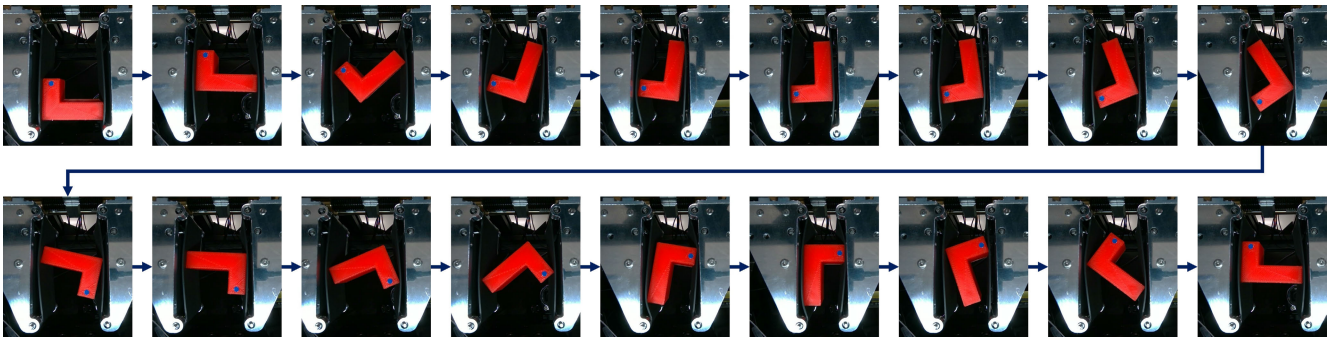

(a) Sequential in-hand manipulation to rotate an object to 1 revolution, whose cross section has an asymmetrical convex shape and high aspect ratio.

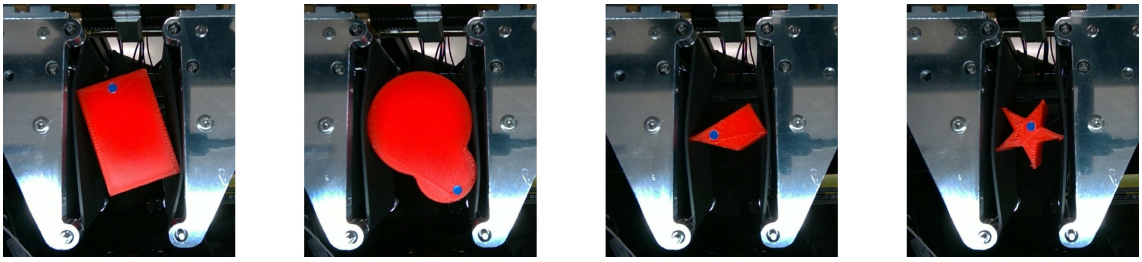

(b) Some examples of the variously shaped and sized objects to which the proposed method can be applied.

FIGURE 1. Overview of the motion and objects on which the proposed method is focused. (a) Targeted motion to rotate an object through a large range. (b) Some examples of objects dealt with by using this method.

the hand workspace is a major challenge of this task. The challenging motion and objects dealt with in this paper are shown in Fig. 1.

There are many studies for IHM with the underactuated, soft or multiple fingered hands [6], [7], [8], [9], [10], [11], [12], [13], [14], [15], [16], [17], [18], [19], [20]. Since these hands can conform to the shapes of various objects, the grasping capability can be satisfied. On the other hand, to achieve a large range of motion, "*regrasping*" is required due to the lack of the manipulability of these hands. *Regrasping* is a motion of releasing a/some finger(s) away from part of the object surface and then contacting it at another part [1], [2]. For these motions, the control scheme is complicated and the sensing requirements are also quite high and may fail. It is more efficient and robust to achieve IHM seamlessly, without regrasping.

To achieve high manipulation capability, robotic hands with active surfaces have been proposed. Active surfaces [5] refer to the movable components such as belts [21], [22], [23], [28], [29], [30], [31], [32] or rollers [24], [25], [26], [27] on a finger, which can continuously rotate or translate the grasped object. While the objects with simple shapes like cubes or cylinders can be easily manipulated through a large range of motion by active surfaces, it is difficult to deal with various shapes of the objects. This is because, the required width of the fingers for maintaining the grasp changes depending on the object shape and orientation during manipulation. When the changes in the required width is large, the fingers may not follow the width, leading to dropping. The main issue is that previous methods [21], [22], [23], [24], [25], [26], [27], [28], [29], [30], [31], [32] have mostly ignored detection of the object's shape and orientation during manipulation. To solve this problem, we previously proposed a visual feedback method using a stereo camera [33]. In our previous method, the fingers and belts were controlled so that the fingers follow the required width, based on the detection of the shape and orientation of a grasped object with a stereo camera. By the previous method, a larger rotation with objects of more variety was achieved. However, almost half of all the tested objects were still dropped from the hand or could not be rotated anymore. These failures occurred because the unwanted rotation was produced by factors other than belts e.g. the grasping force and also the rotation from the belts could not be generated appropriately. To increase the manipulability of objects, it is necessary to cancel the unwanted rotation and allow the belts to produce the appropriate rotation of the object.

In this paper, we propose an in-hand manipulation method for objects with various shapes and sizes through a large range of motion (especially rotation), by a robotic gripper equipped with belts as active surfaces. The purpose of the method is to increase the variety of the manipulatable objects by enabling the fingers to follow the object and generating the appropriate rotation. We use a two-fingered parallel gripper equipped with soft-rubber conveyor belts. To obtain the information for controlling the fingers and belts, a stereo camera is attached to the hand. First, the shape and orientation of the grasped object are extracted from an image. Based on the extracted information, the switching of contact points between the object and the belts is predicted. According to the prediction, the angular velocity of the object is determined so that the fingers can follow the object so as not to drop it. Assuming

that the object will be rotated at the desired angular velocity, it is predicted where the contact points and the centroid of the object will move by the next frame. Then the belts are deflected based on the shape and orientation of the object to both canceling the undesired rotation by anything other than the belts and generating appropriate rotation from the belts. Depending on the predicted information in the next frame and the deflection, the fingers are controlled. Finally, the control commands for the belt velocities are given so that the object rotates at the desired velocity even if factors other than the belt contribute to the rotation. The validity of the proposed method is verified through experiments to rotate 32 samples (16 shapes and 2 sizes) and 12 real-world items through 1 revolution.

The novelties and contributions of the proposed method are as follows:

- Increasing the variety of objects with different shapes and sizes by detecting of its shape, orientation and the changes in the contact points from a stereo camera.
- Extending the rotational range by controlling the belt and finger velocities, and producing the appropriate rotation by deflecting the belts and canceling the undesired rotation.
- Seamless and continuous manipulation for variously shaped and sized objects and a larger range of rotation by conveyor belts (active surfaces) without regrasping or any complex control schemes.

The paper is organized as follows: first, we review the state-of-the-art IHM approaches in Section II. The focused challenges are indicated in Section III. The hardware component and the robot coordinate system we assume are illustrated in Section IV. In Section V, the details of the proposed sensing and control methods are described. Section VI shows the experiments using various objects with large ranges of manipulation. Moreover, the proposed method is also applied to the real-world objects as described in Section VII. Through these experiments, the effectiveness of the proposed method is explored. Finally, the paper is concluded and future works are described in Section VIII.

II. RELATED WORKS

As mentioned above, IHM requires both grasping and manipulation capabilities. From each aspect, state-of-the-art approaches to IHM are introduced in this section.

Focusing on the grasping ability when responding to variously shaped objects, robotic hands with deformable [6], [7] or underactuated fingers [8], [9], [10] have been developed. In these hands, the motion can be changed to follow the shape of the object. Thanks to these changes, the contact region between the surfaces of the grasped object and the finger can be increased so as not to drop the object. Further, increasing the contact region also contributes to the manipulation capability, because the force from the increased region can be effectively applied in the direction required to manipulate (especially rotate) the object. Meanwhile, Spiers et al. [11] presented a robotic finger configuration that can change its friction surface depending on the manipulation mode: sliding or rolling the grasped object. Increasing the grasping force switches the surface to high friction and contributes to the rotation of the object. Due to the high-friction surface, the contact between object and surface can be maintained without the slippage or ejecting the object from the hand. However, since these hands cannot manipulate the object with high degrees of freedom (DOFs), the range of the manipulation is limited. To achieve a high range, it is necessary to use environments outside the hand workspace [12], [13], [14]. Temporarily placing the object onto a table or pushing it against a wall allows the hand to change its area of contact with the object, or to pivot the object, resulting in manipulation capability beyond the DOF of the hand itself. However, such methods require complex strategies, making the motion longer. Without using extrinsic environments, control systems for robotic hands with high DOFs have also been proposed [15], [16], [17]. Systems with soft fingers to stably grasp the object were also investigated [18], [19], [20]. Even though the manipulation can be carried out within the hand, a "*regrasping*" motion is still necessary. As previously noted, *regrasping* is behavior to change the contact regions by releasing the object and grasping it again with another part of the object surface. Realizing seamless and continuous manipulation without regrasping or using complicated schemes of control remains a challenge.

To overcome these challenges, a robotic hand with "*active surface*" has attracted interest. The active surface consists of rolling components, such as belts or rollers, that are usually attached to the finger surface. Although this configuration is different from conventional, human-like hands, it is considered appropriate for continuous and uncomplicated IHM. The manipulation to pull in (translate) the object has been accomplished with versatility, as described by Morino et al. [21], Nishimura et al. [22] and Kakogawa et al. [23], by actuating both active surfaces on the fingers in the same direction. To extend the usage to rotation, Yuan et al. [24] constructed a three-fingered hand with driven rollers on each fingertip. Controlling each finger and roller independently achieved IHM with 6 degrees of freedom. They also evolved the rollers into a spherical form and achieved continuous manipulation in [25]. While the fingers are fully controlled to grasp the object during rotation, the configurations to passively follow the object shapes have been widely adopted. The configurations with passively moved components allow a stable grasp of the object without the precise control achieved by using tactile sensors. Moreover, because it is possible for the active surface to passively fit the object shape, the desired rotation may be appropriately generated by the active surface. Tahara et al. [26] proposed a manipulation method for the dual-fingered hand with torsional fingertips. The fingertips, made of soft polyurethane, can deform so that the contact region between the surfaces of the object and the fingertips is increased. A hand with both rolling and passively bending

underactuated fingers was presented by Gómez-de-Gabriel and Wurdemann [27]. Also, the two-fingered hand advanced by Tincani et al. [28] consists of an underactuated gripper with conveyor belts. Thanks to the underactuated components, the fingers can change their configurations so as to grasp the object by following its shape. Additionally, by using underactuated fingers with a belt and rollers, an approach to adaptively grasp the object was proposed in [29] and [30]. Because of the adaptability of the underactuated design, IHM can be repeatedly achieved without a priori knowledge about the object. Govindan et al. [31] also created a unique hand with belts on two fingers that can be deflected to a large extent. Because the deflection passively varies according to the object shape, the hand fully envelopes and stably grasps the object. Cai et al. [32] utilize a soft hand whose surfaces are wrapped with conveyor belts. As the soft fingers are deformed by the grasping force, so as to fit the object shape, both a stable grasp and continuous manipulation can be realized simultaneously. Though a variety of hand configurations have been designed with simplified control, only cubes, cylinders, and similarly shaped objects could be manipulated in a high rotational range, i.e., more than 1 revolution. However, in cases where IHM is required, manipulating a wider variety of shapes is a challenge. Due to the following challenges, it is difficult to manipulate objects of various shapes through a large range of motion.

III. CHALLENGES

As discussed in [24] and [32], both grasp and manipulation capabilities are restricted by the shape of the object, even when active surfaces are used. Reference [11] demonstrated that varying the friction of the finger surface prevents slippage of some objects even if their orientation has been continuously changed during the rotation. In light of these considerations and ideas, this subsection describes some situations when both capabilities decrease and the strategies in those situations. In this research, we attempt to develop a robust control system for a two-fingered, belt-equipped robotic hand as shown in Fig. 1. We focus on two challenges: dropping the object and the difficulty of rotation.

A. THE SITUATION IN WHICH THE GRASPED OBJECT IS EASILY DROPPED

Here, we focus on two situations in which the object is likely to be dropped and the grasp stability decreases.

1) THE SITUATION IN WHICH THE FINGER CANNOT FOLLOW THE WIDTH REQUIRED NOT TO DROP THE OBJECT

One situation is when the finger cannot follow the width required not to drop the object, as mentioned in our previous work [33]. Fig. 2(a) shows an example in which an object is rotated in a clockwise direction using a two-fingered parallel gripper equipped with belts. In the figure, the cross-sectional shape of the object is drawn as a red rectangle. The object is rotated in the direction indicated by the arced white arrow. The motion of the fingers and belts is illustrated by the red and green arrows, respectively. The fingers are closed so as not to drop the object. Here, it does not matter whether the fingers are moved by a torque control, some underactuated configurations to passively fit the fingers to the object shape, or a full position/velocity control. That is, the focused problem can occur whichever control method is applied. The belts are moved to rotate the object in the direction indicated by the arced white arrow.

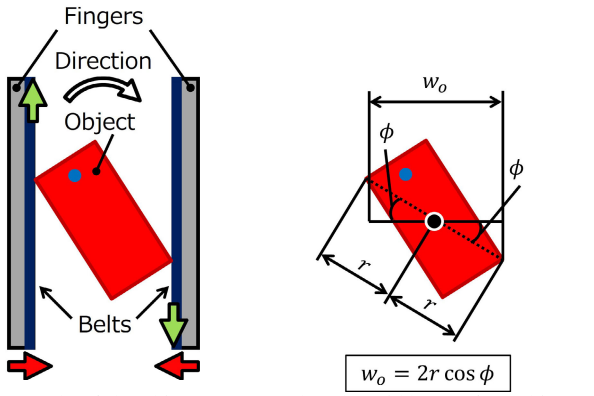

(a) Example of the object's rotation by a two-fingered parallel gripper equipped with belts.

(b) The width w_o of an object with a rectangular cross section.

FIGURE 2. Example of the required movements of the belts and fingers to rotate and prevent dropping of the object. The belts are moved as indicated by the green arrows, to rotate the object in the direction indicated by the arced white arrow in (a). As described by the red arrows, the fingers close so that the width between them is w_o.

In Fig. 2(b), the notable geometric information for this object is described. w_o indicates the horizontal distance between both contact points between the surfaces of the object and each belt. r is the rotational radius of the object computed by half the distance between both contact points. The rotational center is depicted as a black circle. ϕ is calculated as the angle between the line connecting both contact points and the horizontal axis. Based on the rotational radius r and angle ϕ, w_o is calculated as the multiplication of $2r$ by $\cos\phi$. For a stable grasp, the fingers should open or close to tailor their width to w_o, which is varied by the rotational radius r and angle ϕ. Because w_o varies in proportion to $\cos\phi$, even when the object rotates at the constant angular velocity, the changes in w_o are not constant. Therefore, it is possible that w_o changes so significantly that the fingers cannot follow the width because of the dynamic characteristics of the actuators. The maximum displacement of the fingers between one unit of time is given by the performance, which depends on the current velocity and the maximum acceleration of the actuators. That is, when the changes in w_o in one frame exceed the maximum displacement, the object may be dropped. Moreover, the closer the switching of the contact point to another point is, the larger the angle ϕ is and the larger the changes in w_o are. Therefore, the object is most likley to be dropped just before the contact point switches. To prevent dropping, based on recognizing when the current contact point will be switched

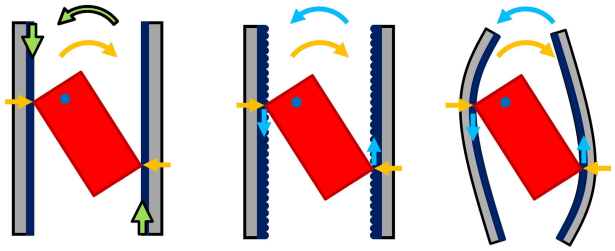

FIGURE 3. The strategies to resist the rotation caused by the grasping force when it is desired to be kept in a certain orientation. (Left) Canceling the rotation due to the forces by controlling the belt in the opposite direction. (Center) Using the belt with a high-friction surface to prevent rotation by the grasping force. (Right) Producing the tension of the belt by deflecting or deforming the flexible belts.

to another point, adjusting the angular velocity of the object enables the fingers to follow the required width.

2) THE SITUATION IN WHICH THE ROTATION IS PRODUCED BY FACTORS OTHER THAN THE ACTIVE SURFACES

Another situation is dropping due to the rotation produced by factors other than the belt (active surfaces), especially the grasping force (which is dominant). When attempting to rotate the object to an arbitrary angle using the belts, the object rotates more than expected because the grasping force also contributes to the rotation. Furthermore, the rotation by the grasping may occur not only when the belts move but also when the belts are stopped. To simplify the problem, here, a situation is assumed in which keeping the rotation of the object in a certain orientation is attempted. In this situation, three examples of strategies to deal with rotation due to the grasping force are shown in Fig. 3. All strategies are designed to resist the rotation by the grasping force. In the figure, the object, fingers and belts are shown by the red, gray and navy blue parts respectively, as in Fig. 2(a). The horizontal orange arrows describe the grasping forces. The rotation caused by them is depicted by the arced orange arrows. Note that although the rotations are also caused by factors other than those shown, such as friction or reaction forces, only the rotation due to the grasping force and that related to the strategy are illustrated in the figure.

In the strategy shown in the left part of the figure, the directions of the belt movement and rotation caused by the belts are indicated by vertical and arced green arrows, respectively. By controlling the belts so as to generate rotation in the opposite direction of the rotation due to the grasping force depicted by the arced orange arrow, the rotation is canceled to maintain the object orientation. In the center image, the waved surfaces of the belts indicates that these friction is high. The high friction of the belt surface contributes to preventing the object from rotating too much and being dropped, as adopted in [11]. The vertical blue arrows represent the friction forces, and the arced blue arrow is the moment from them. In the strategy on the right, the belts are deflected or deformed as in [31] and [32]. The tension from the deflected belts or the force from the expanded contact region due to deformation (the vertical blue arrows) can produce the rotation (the arced blue arrow) in the direction drawn in the figure.

When both the rotation due to the grasping force (each arced orange arrow) and the rotation in the direction indicated by the green or arced blue arrow in each strategy have comparable magnitude, the object can remain within the hand workspace and does not fall. In this paper, the first and third strategies (i.e., the left and right images in Fig. 3) are introduced. These strategies are applied by adjusting their dependence according to the shape and orientation of the objects. The second strategy will be considered in future works.

B. THE SITUATION IN WHICH THE GRASPED OBJECT IS DIFFICULT TO MANIPULATE

In this subsection, the situation in which it is difficult to manipulate a grasped object and the manipulation capability decreases is detailed. Fig. 4(a) shows an example of this situation, where an object is in an orientation in which it is difficult to rotate. The white arrows indicate the direction in which the object (described in red) is to be rotated. The fingers (gray parts) are controlled to accommodate changes in the required width, as indicated by the horizontal red arrows. The vertical green arrows indicate the movements of both belts (navy blue parts) to rotate the object in the desired direction.

In Fig. 4(b), the arced green arrow shows the rotation caused by the belts. The components of the belt movements that contribute to the object's rotation are illustrated by the straight green arrows. The diameter of the rotation is depicted as a dotted line that connects both contact points between the surfaces of the object and belts. The rotational center is depicted as a black circle and is the midpoint of the dotted line. As indicated in the figure, when the slope of the dotted line is large (nearly vertical), the straight green arrows are short. That is, it is difficult for the belts to contribute to the rotation in the drawn situation, and only a small rotation is produced. Here, the slope is varied by not only the object's orientation but also its shape. If the object is not rectangular but square, the slope is smaller (more horizontal) than the drawn one, even though its orientation is the same. Furthermore, the rotation produced by factors other than the belts also occurs in this situation, in a direction that cancels the rotation by the belts. Therefore, when the rotation by the belt is canceled and the object cannot be rotated, the manipulation capability is also limited, though the object is not dropped. This occurs even if the finger can open to the estimated width, which is calculated assuming the object rotates as desired. Moreover, when the fingers open but the object does not rotate, the width required to grasp the object is smaller than estimated, which may cause the object to fall from the hand or slip on the surface of the belt. Thus, the grasping capability is also possible to decrease.

In this case, both increasing the belt velocities so as not to be canceled and changing the friction and the deflection or

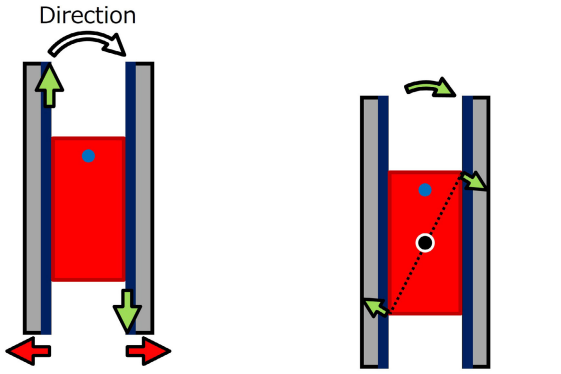

(a) Example of the situation in which the object is difficult to rotate, even without dropping it.

(b) The rotation of the object drawn in (a) due to the movement of the belts.

FIGURE 4. Example of a challenge situation in which the manipulation capability can decrease. (a) Situation in which the object is in an orientation that makes it difficult to rotate, even though the belts and fingers are moved to rotate it. (b) Example of small rotation caused by the movements of the belts.

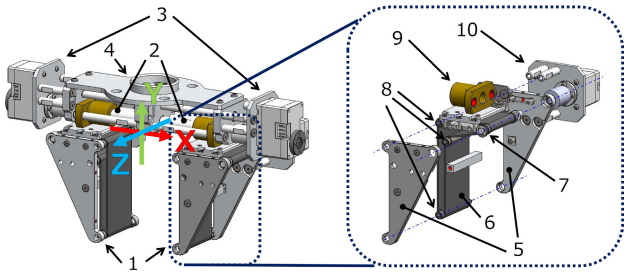

1. Fingers
2. Lead screws
3. Finger motors connected to the lead screws 2
4. Base part connectable to a robotic arm (Not shown)
5. Frames
6. Circular belt
7. Drive shaft to circulate the belt 6
8. Idler shafts supporting the belt 6
9. Nut for lead screw 2
10. Belt motor connected to the drive shaft 7

FIGURE 5. The mechanical component used in the proposed system and the coordinate system for control.

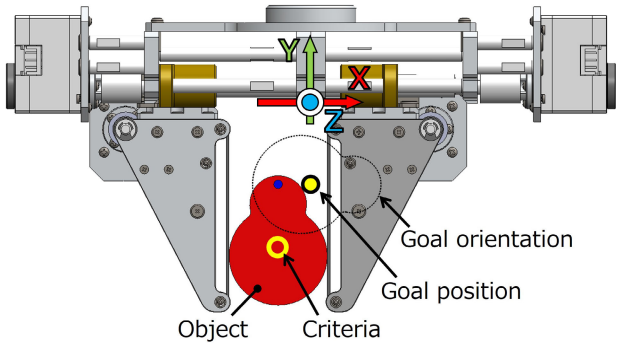

FIGURE 6. The robot coordinate system and the definition of the goal.

deformation of the belts to produce a large rotation are valid strategies. These strategies are similar to ones explained in Sub-subsection III-A2 and shown in Fig. 3. Especially with deflecting or deforming the belts, the difference between the estimated and actually required width of the fingers also can be absorbed, as a feature of the robot using soft materials.

IV. MECHANICAL DESIGN AND COORDINATE SYSTEM

In this section, the mechanical design of the robotic hand and the coordinate system are described.

A. MECHANICAL DESIGN

As in our previous work [33], we use a two-fingered parallel gripper with conveyor belts (active surfaces) as a robotic hand. As mentioned in Section II, the active surfaces allow for seamless and continuous rotation of the object and high manipulation capability, i.e., more than 1 revolution. No special configuration (e.g., underactuated or compliant component) is introduced other than the active surfaces made by an elastic material, which is utilized in the related works [23], [28], [29], [30], [31], [32] as well.

Fig. 5 shows the details of the hand configuration. Each finger (1) is controlled by the respective motor (3) via a nut (9) on the upper side of the finger and a lead screw (2) connected to the motor. The surface of each finger is wrapped with a circular belt (6). Each belt is controlled via the drive shaft (7) by a motor (10). The belt is also supported by frames (5) at the front and back of the unit (1) and three idler shafts (8) so as not to become loose. Therefore, the grasped object can be translated with respect to the Y (vertical) axis and rotated around the Z axis by controlling the belts. Additionally, the hand can be connected to a robotic arm on the base (4).

Using this hand, an object can be grasped by being pinched between both belts. When both fingers are moved in same direction while maintaining the grasp, the object can be translated along the X (horizontal) axis. As previously mentioned, controlling both belts so that they move in the same direction enables the object to be translated along the Y axis. The object can be rotated around the Z axis by moving the belts in different directions. The coordinate system consisting of these X, Y, Z axes is called the robot coordinate system in this paper.

This hand is not equipped with a tactile sensor, as it is difficult to design and fabricate sensors that can be attached to a moving belt. A stereo camera is utilized as an external sensor. The camera is mounted on the robotic hand and arranged so that the hand workspace directly in front of it can be captured.

B. COORDINATE SYSTEM

The robot coordinate system viewed from the front of the robotic hand is described in Fig. 6. In the figure, the criterion for the position of a grasped object is indicated by a hollow yellow circle. Additionally, the goal position (solid yellow circle) is given as X_{goal} and Y_{goal} with respect to the X and Y axes, respectively. The orientation is calculated as the angle

around the Z axis. Manipulation is implemented to align the criterion with the goal position and the orientation of the object with the goal orientation θ_{goal}.

V. PROPOSED CONTROL SYSTEM

This section details the control strategies using a camera image to achieve a system that can manipulate various objects through a large range of motion.

A. OVERVIEW OF THE CONTROL SYSTEM

The flow chart of the proposed control system is shown in Fig. 7. First, a color image is acquired by a stereo camera. The contour of the grasped object is obtained using color information from the image. From the contour, the position and orientation of the object are calculated. Then the contact points between the surfaces of the object and each belt and the vertex that will be contacted next are detected. The angle between the line connecting both points and the belt (the vertical axis) is calculated. Here, the angle shows how much rotation is required to switch the contact points. Based on the calculated angle, the angular velocity of the object in the next frame is determined so as to overcome the challenge mentioned in Sub-subsection III-A1. Additionally, assuming that the object rotates at the desired velocity without slippage, the shape in the next frame is predicted. Then, from the present image, the angle between the line connecting the contact point and the centroid of the object and the horizontal axis is calculated. According to this angle, the amount of belt deflection is modulated. This is the strategy shown on the right in Fig. 3 to deal with the challenges referred to in both Sub-subsection III-A2 and Subsection III-B. Through the deflection, the tension from the belts or the force from the expanded contact region can occur and induce the rotation. The deflection is produced by controlling the fingers so that the belts are pressed onto the object. The command for the fingers is calculated to both follow the predicted shape and produce the deflection. Next, the angular velocity of the object generated by the current belt velocities is calculated, assuming that no slippage occurs between the surfaces of the object and each belt. The difference between the current angular velocity of the object and the calculated angular velocity from the belts is computed as the angular velocity from the others (mainly the grasping force). The desired velocity of the belt is calculated to rotate the object at the desired angular velocity while canceling the rotation due to factors other than the belts. This is the strategy shown on the left in Fig. 3 to address the challenges mentioned in both Sub-subsection III-A2 and Subsection III-B. Finally, both the fingers and the belts are controlled based on the calculated commands. The above procedures are implemented repeatedly in every frame until the object reaches the goal position and orientation, given as the position X_{goal}, Y_{goal} on the X and Y axes and the orientation θ_{goal} around the Z axis.

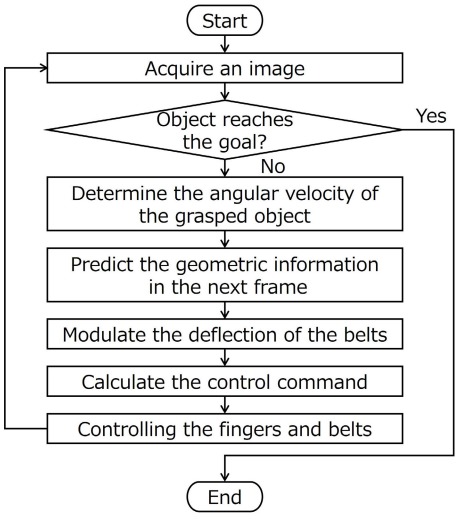

FIGURE 7. The flow chart of the proposed control system.

B. DETERMINATION OF THE ANGULAR VELOCITY

This section details the process of determining the desired angular velocity of the object in the next frame by using a camera image. As mentioned in Sub-subsection III-A1, even if the object is rotated by a fixed angle during a frame (unit of time), the changes in the required width of the fingers are varied depending on the object's shape and orientation. The possibility of dropping the object increases the closer it is to a contact-point switch. For stable in-hand manipulation, the angular velocity of the object should be varied based on the switching of the contact points. That is, the velocity is slowed down according to the switching so that the fingers can follow the required width.

In order to achieve this control, we detect the angle at which the contact points change via image processing. First, a contour of the cross section of the grasped object is extracted from a color image based on the given color information of the object. Fig. 8(a) shows an example of an input image, and the contour is depicted as a pale blue line in Fig. 8(b). Next, the centroid of the region enclosed by the contour is calculated. It is defined as the current centroid $c_{pos}(t)$ of the object and drawn as a yellow circle in Fig. 8(c). Here, $c_{pos}(t)$ is the criterion of the object's position, i.e., the translation of the object is implemented to align $c_{pos}(t)$ with the goal position X_{goal} and Y_{goal}. Next, polygon approximating the contour is produced via the Douglas–Peucker algorithm [34]. Since the concave parts of the object are not contacted by the belt on the parallel gripper, a convex hull of the polygon is computed using the Quickhull method [35] as indicated by the green outline in Fig. 8(c). Then the leftmost and rightmost vertices of the hull are regarded as the present contact points of the respective left and right side, $p_{cl}(t)$ and $p_{cr}(t)$. These are shown as blue and pink circles in Fig. 8(c), respectively. Additionally, the rotational center $c_{rot}(t)$ is computed as the midpoint of both the contact points. $c_{rot}(t)$ is depicted as a

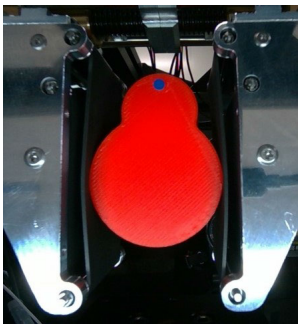

(a) The input image.

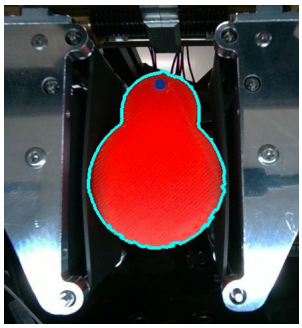

(b) Extraction of the contour of the cross section, shown as a light blue line.

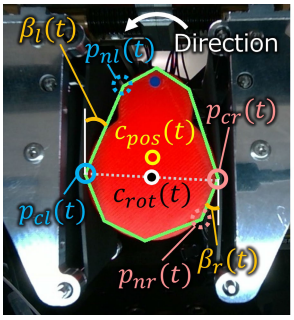

(c) The contact information when rotating in a counterclockwise direction.

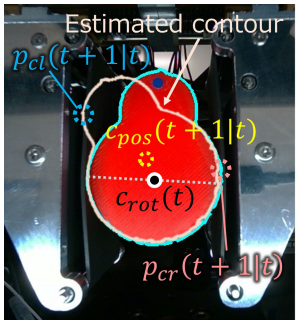

(d) Prediction of the geometric information in the next frame.

FIGURE 8. The process of calculating the required information. The angle $\beta(t)$ between the current and next contact points, $p_c(t)$ and $p_n(t)$, is calculated for use in controlling the belt. By rotating the contour, both the centroid and the contact point in the next frame are estimated as $c_{pos}(t+1|t)$ and $p_c(t+1|t)$, respectively.

black circle in the figure. Next, the points where the belts will contact next if the rotation continues are estimated from the vertices of the hull, namely the next contact points $p_{nl}(t)$ and $p_{nr}(t)$. Considering the direction of the rotation, the neighbor vertices of both present contact points ($p_{cl}(t)$ and $p_{cr}(t)$) are defined as the next contact points. In the figure, the direction of the rotation is indicated as an arced white arrow: a counter-clockwise direction. The next contact points ($p_{nl}(t)$ and $p_{nr}(t)$) are depicted as dotted blue and pink circles, respectively. Finally, the angle required to rotate to change the contact point is detected. It is calculated as the angle between the line connecting the present and next contact points and the belt (the vertical line). The calculated angles for the respective left and right side are named $\beta_l(t)$ and $\beta_r(t)$ and drawn as an arced orange line in the figure.

If the angles $\beta_l(t)$ and $\beta_r(t)$ are small, it is easy to drop the object, because the required width of the fingers can be changed easily and to a large degree. Conversely, when the angles $\beta_l(t)$ and $\beta_r(t)$ are large, it is easy to rotate the object without dropping it. Therefore, the proposed method uses $\beta_l(t)$ and $\beta_r(t)$ to determine the angular velocity of the object.

Meanwhile, the maximum displacement of the fingers and belts during one frame (unit of time) are given by the dynamic characteristics of the motors. Considering the dynamic characteristics, the maximum rotational angle $\Delta\theta_{max}$ by the next frame is given as

$$\begin{aligned} R(t) &= \frac{\|P_{cl}(t) - P_{cr}(t)\|_2}{2}, \\ \Delta\theta_{f,max}(t) &= \cos^{-1}\left(\frac{f(t)+\Delta f_{max}(t)}{R(t)}\right) - \cos^{-1}\left(\frac{f(t)}{R(t)}\right), \\ \Delta\theta_{b,max}(t) &= \sin^{-1}\left(\frac{b(t)+\Delta b_{max}(t)}{R(t)}\right) - \sin^{-1}\left(\frac{b(t)}{R(t)}\right), \\ \Delta\theta_{max}(t) &= \min\left(\Delta\theta_{f,max}(t), \Delta\theta_{b,max}(t)\right), \end{aligned} \tag{1}$$

where $R(t)$, $P_{cl}(t)$, and $P_{cr}(t)$ are the rotational radius and both contact points in the robot coordinate system; $\Delta\theta_{f,max}(t)$ and $\Delta\theta_{b,max}(t)$ are the maximum angles to rotate the object allowed by the finger and the belt, respectively; $f(t)$ and $b(t)$ are the current position of them; and $\Delta f_{max}(t)$ and $\Delta b_{max}(t)$ are the maximum displacement of them during the processing time Δt given by their dynamic characteristics, i.e., the current velocities and the maximum accelerations of the actuators. Note that, by considering the left and right fingers and belts, and the direction of the rotation, (1) is calculated.

Based on both of the angles, $\beta_l(t)$ and $\beta_r(t)$, and $\Delta\theta_{max}(t)$, the desired angle $\Delta\widehat{\theta}(t)$ of the object by the next frame is determined as follows:

$$\begin{aligned} \Delta\widehat{\theta}(t) &= \min(K_\theta\beta_l(t), K_\theta\beta_r(t), \Delta\theta_{max}(t), \Delta\theta_{goal}(t)), \\ \Delta\theta_{goal}(t) &= \theta_{goal} - \theta(t), \end{aligned} \tag{2}$$

where K_θ is the gain value of the rotation, $\Delta\theta_{goal}(t)$ is the difference between the goal angle θ_{goal} and the present orientation of the object $\theta(t)$. The desired angular velocity $\hat{\dot{\theta}}(t)$ is calculated by differentiating $\Delta\widehat{\theta}(t)$ with time.

Here, the angular velocity $\hat{\dot{\theta}}(t)$ depends on not only $\Delta\theta_{max}(t)$ but also $\beta_l(t)$ and $\beta_r(t)$, for the following three reasons. First, the rotational radius of the object can change when the contact point changes. The angular velocity may be fast even near the switching of the contacts if the angular velocity is calculated without the contact information. That is, the rotational radius and the required width can change significantly before and after one frame because of the switch with fast angular velocity. Because of this, the fingers may not follow the changes in width. Near the switching, slowing down the angular velocity keeps small changes in the width due to the changes in the radius. The second reason is to retain the grasp even if there are errors in the image processing to calculate the required width of the fingers. The closer the switching is, the larger the effect from the detection error of the width is. When $\beta_l(t)$ and $\beta_r(t)$ have a small value, changing the width gradually by slow rotation allows the decrease of the effect of the error. The third reason relates to the effect of the rotation caused by factors other than the belts. As detailed in Subsection V-D, the rotation induced by factors other than the belts occurs, and the effect of it varies based on the orientation of the object. This rotation is likely to be large when the switching of the contact points

is close, causing the object to be dropped or not to rotate anymore. Therefore, the strategies to estimate and cancel this rotation in every frame are adopted in the proposed method, as detailed in Subsection V-D and V-E. However, if the angular velocity is fast near the switching, this rotation can be changed significantly. Because the error in estimating this rotation increases due to the large change, the effectiveness of the strategies may decrease. In contrast, the small changes in orientation with low velocity decrease the effect from the error. Using $\beta_l(t)$ and $\beta_r(t)$ to determine the angular velocity helps to adjust the effect of the estimation error of rotation by factors other than belts and keeps the effectiveness of the proposed strategies.

C. PREDICTION OF THE GEOMETRIC INFORMATION IN THE NEXT FRAME

In this section, the geometric information of the object in the next frame is predicted. Through the process detailed in Subsection V-B, the angular velocity of the object is determined to enable the finger to follow the required width. Therefore, the fingers should be controlled to stably grasp the object according to the object information: the contact points and the centroid of the object. However, the process to detect the object information in the above section is based on an image in the present frame. Using information about the present state of the object results in a feedback control of the fingers that has a primary delay. Depending on the amount of delay per unit of time, the object may fall from the hand, even though the fingers can move to the commanded position. Therefore, as a strategy to prevent this, a feed-forward control is executed by estimating the geometric information of the object in the next frame.

To estimate the object's geometric information in the next frame, the object contour is rotated to the desired angle $\Delta\widehat{\theta}(t)$. By rotating each point $p_i(t) = (u_i(t), v_i(t))^\top$ on the object contour to the angle $\Delta\widehat{\theta}(t)$ around $c_{rot}(t) = (u_{rot}(t), v_{rot}(t))^\top$, $p_i(t)$ is estimated to be moved to $p_i(t+1|t)$ with following equations:

$$\begin{aligned} l_i &= \|p_i(t) - c_{rot}(t)\|_2, \\ \alpha_i(t+1|t) &= \tan^{-1}\left(\frac{v_i(t) - v_{rot}(t)}{u_i(t) - u_{rot}(t)}\right) + \Delta\widehat{\theta}(t), \\ p_i(t+1|t) &= l_i \begin{pmatrix} \cos\alpha_i(t+1|t) \\ \sin\alpha_i(t+1|t) \end{pmatrix} + c_{rot}(t). \end{aligned} \tag{3}$$

Here, l_i is the length of the line connecting each point $p_i(t)$ to the rotational center $c_{rot}(t)$, and $\alpha_i(t+1|t)$ is the estimated angle between the line and the horizontal axis in the next frame.

The estimated contour is drawn in Fig. 8(d) as a pale pink line. Then the leftmost and rightmost points of the estimated contour are detected as $p_{cl}(t+1|t)$ and $p_{cr}(t+1|t)$, respectively. As well as the current centroid $c_{pos}(t)$, the centroid $c_{pos}(t+1|t)$ of the object in the next frame is calculated from the estimated contour. $c_{pos}(t+1|t)$ is depicted as a dotted yellow circle in the figure. These points are used as predicted object information to calculate the control commands explained in Subsection V-E. The estimated contact points $p_{cl}(t+1|t)$ and $p_{cr}(t+1|t)$ are used for the width of the fingers. The centroid $c_{pos}(t+1|t)$ of the estimated contour is used for both fingers and belts to translate the objects.

D. MODULATION OF THE DEFLECTION

This subsection presents a strategy to increase both the grasp and manipulation capability, focusing on the rotation caused by multiple factors. As detailed in Sub-subsection III-A2, there may be a situation in which the rotation due to factors other than the belts is significant enough to cause the object to be dropped. Additionally, as mentioned in Subsection III-B, the belts may be difficult to rotate the object, even when the fingers are moved to follow the required width. These situations occur because it is difficult to produce the proper rotation of the object. The difficulty is related to both the object shape and orientation. In this subsection, first, the condition under which the proper rotation is so difficult to be produced that the object is easily dropped or is difficult to rotate is detailed. To grasp and manipulate the object under this condition, the belts are deflected to generate the tension or the force required for the proper rotation. Furthermore, by deflecting the belts, the difference between the estimated and actual required width of the fingers can be absorbed, as a feature of the robot using soft materials. Then the strategy for when to deflect the belts and how large a deflection is generated is introduced.

Fig. 9 shows the rotation caused by the grasping force, as an example of a factor other than the belts. Note that the figures in this subsection do not show any free body diagram but show the produced force or rotational moment by one factor, which is the focus in each explanation. In Fig. 9(a), an example of the situation in which the object is grasped are stopped is drawn. Note that, it is assumed that the belts are stopped for simplification. In this situation, only the grasping forces F as factors related to the rotation are illustrated using orange arrows. Of course, though there should be forces other than the grasping force, such as friction or reaction forces, only the grasping forces are focused on here for the purpose of explanation. As a parallel gripper is used, the grasping forces are assumed to be applied horizontally. In this situation, the rotation may occur due to the forces, as shown in Fig. 9(b). The components of the grasping forces that contribute to the rotation are represented by the straight orange lines. These components contribute to the rotation by producing the rotational moment around the rotational center (black circle) in the direction depicted by the arced orange arrow. Here, ϕ is the angle between the horizontal axis and the line connecting both contact points, indicated by the dotted line. The amount of each component of the grasping force is calculated using $F\sin\phi$. Therefore, the larger ϕ is, the more the acceleration of the rotation caused by the forces, even when keeping the grasping force F at a constant value.

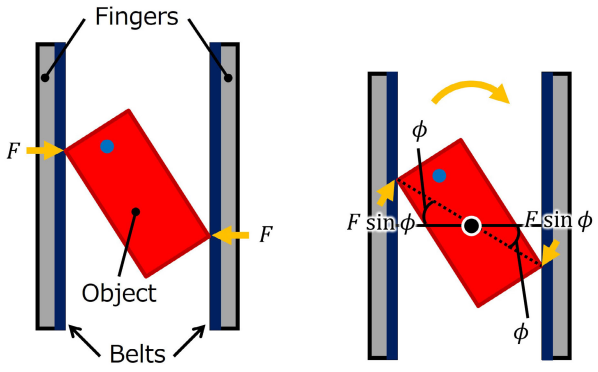

(a) Example of the grasping force F occurring on a grasped object

(b) The rotation caused by the force drawn in (a)

FIGURE 9. Example of the rotation caused by the grasping force alone when the belts stop moving. (a) Situation in which the grasping forces F are applied. (b) The rotation produced by the grasping force F.

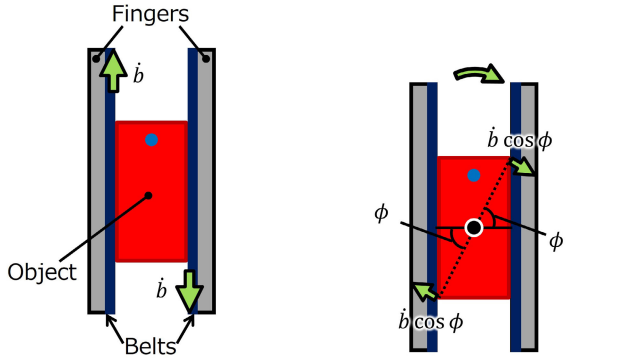

(a) Example of grasping an object when the belt moves at the velocity $\dot{b}$.

(b) The rotation caused by the movements of the belt in the situation in (a).

FIGURE 10. Example of the rotation caused by the belts alone. (a) Situation in which the belts move at the velocity $\dot{b}$. (b) The rotation produced by the movements of the belts.

On the other hand, the rotation due to the belt movements is shown in Fig. 10. Fig. 10(a) is an example of the situation in which the belts move at the velocity $\dot{b}$. The vertical green arrows represent the directions of the belt movements. In the figure, only the movements of the belts are focused on, and finger movements in a similar situation are illustrated in Fig. 4(b). Fig. 10(b) describes the rotation of the object caused by the belts in the situation in Fig. 10(a), indicated by an arced green arrow. The velocity of the belt contributes to the rotation by producing the angular velocity of the object. However, because the direction of the belt movement is vertical, the angular velocity may be difficult to produce due to the angle ϕ. The components of the belt velocities that relate to the angular velocity are calculated using $\dot{b}\cos\phi$, as depicted by the straight green arrows. Therefore, the larger ϕ is, the more difficult the belts are to contribute to the rotation of the object, even when the belt velocity is constant at $\dot{b}$.

Thus, we conclude that the difficulty to rotate the object depends on the amount of ϕ, because according to ϕ, the object may be easy to drop or difficult to rotate. Here, the angle ϕ is calculated as follows:

$$\phi = \cos^{-1}\left(\frac{w_o}{2r}\right), \tag{4}$$

where w_o and r are the variables shown in Fig. 2(b). Here, the rotational radius r is determined by the shape of the object. w_o is varied according to the orientation, even if the rotational radius is constant. That is, it depends on both the shape and orientation of the object, whether the proper rotation of the object can occur or not.

In this paper, so as not to drop the object and to manipulate it appropriately, the belt is deflected as previously described in the right image in Fig. 3. Deflecting the belt causes the tension in the direction to cancel the rotation caused by the grasping force. Simultaneously, likely due to the soft robotic hands, the belt is deformed to fit the shape of the object. Furthermore, the deflection and deformation help to absorb the difference between the estimated and actual width required of the fingers so that the object is not dropped from the hand. In particular, the more difficult it is for the proper rotation to occur, the larger the difference is. Considering both the condition under which the proper rotation is difficult to produce and these properties of deflection and deformation, the amount of the deflection $\delta_{deflect}$ is defined as follows:

$$\delta_{deflect} = \delta_w \sin\phi, \tag{5}$$

where δ_w is a coefficient given as a fixed value.

E. CALCULATING THE CONTROL COMMAND

As the final process, the control commands are calculated to manipulate the object to an arbitrary position and orientation with 3 degrees of freedom. The commands $\dot{\boldsymbol{q}}(t)$ for the fingers and the belts are described as follows:

$$\dot{\boldsymbol{q}}(t) = \begin{pmatrix} \hat{\dot{f}}_l(t) \\ \hat{\dot{f}}_r(t) \\ \hat{\dot{b}}_l(t) \\ \hat{\dot{b}}_r(t) \end{pmatrix}, \tag{6}$$

where $\hat{\dot{b}}_l(t)$ and $\hat{\dot{b}}_r(t)$ are the command values for the velocities of the left and right belts along the Y axis, and $\hat{\dot{f}}_l(t)$ and $\hat{\dot{f}}_r(t)$ are those for each finger along the X axis, respectively.

In the above sections, the parameters are mostly explained as two-dimensional values, i.e., image coordinates. Hereinafter, the parameters defined in the robot coordinates are utilized with the uppercase letters corresponding to the above lowercase ones, except for each angle and orientation. Additionally, each superscript denotes to which axis the value refers, e.g., C^X_{pos} indicates the X value of the centroid C_{pos}. The calculation of each command is detailed, divided into sections with respect to the fingers and the belts.

1) THE COMMAND FOR THE FINGERS

As also proposed in our previous work [33], the fingers are manipulated using a feed-forward control. In addition to the

system proposed in the previous work, the term of the belt deflection is improved.

The required displacement of the left and right fingers by the next frame are expressed as $\Delta\widehat{f_l}(t)$ and $\Delta\widehat{f_r}(t)$, respectively, and are computed as follows:

$$\begin{pmatrix}\Delta\widehat{f_l}(t)\\ \Delta\widehat{f_r}(t)\end{pmatrix} = K_{f,pos}(X_{goal} - C^X_{pos}(t+1|t))\begin{pmatrix}1\\1\end{pmatrix} + \begin{pmatrix}P^X_{cl}(t+1|t) - f_l(t)\\ P^X_{cr}(t+1|t) - f_r(t)\end{pmatrix} + \begin{pmatrix}\delta_{deflect}\\ -\delta_{deflect}\end{pmatrix}, \quad (7)$$

where $K_{f,pos}$ indicates the gain value of the fingers related to translation. $C_{pos}(t+1|t)$, $P_{cl}(t+1|t)$, and $P_{cr}(t+1|t)$ correspond to the estimated centroid $c_{pos}(t+1|t)$ and the estimated contact points for the respective left and right sides, $p_{cl}(t+1|t)$ and $p_{cr}(t+1|t)$, respectively. $f_l(t)$ and $f_r(t)$ are the present positions of the fingers given by the rotary encoders of each motor.

The control commands for fingers $\hat{f}_l(t)$ and $\hat{f}_r(t)$ are given to divide the displacement $\Delta\widehat{f_l}(t)$ and $\Delta\widehat{f_l}(t)$ by the processing time Δt.

2) THE COMMAND FOR THE BELTS

For calculation of the belt commands, the strategy introduced on the left in Fig. 3 is utilized. In this strategy, the rotation caused by factors other than the belts is canceled. Ideally, the observed rotation of the object is supposed to be equal to the rotation calculated based on the belt movements. In the proposed method, the difference between both rotations is considered to be induced by the other factors (e.g., grasping force). To adjust the rotation to the desired one by canceling the difference, the control commands of the belts are calculated.

First, assuming that no slippage occurs and the rotational radius does not change, the relationship between the rotated angle $\Delta\theta$ of the object and the belt displacement ΔX between one frame is defined as follows:

$$R\Delta\theta = \Delta X, \quad (8)$$

where R is the rotational radius in the robot coordinate system.

Then, based on (8), at the time t, the angle $\Delta\theta_b(t)$ that is expected to be produced by the belt between one frame is calculated as follows:

$$\Delta\theta_b(t) = \frac{\Delta X(t)}{R(t)}, \quad (9)$$

where $\Delta X(t)$ is the displacement of the belt between one frame and $R(t)$ is the rotational radius at the time t.

When the object is observed rotating to the angle $\Delta\theta(t)$ between one frame via camera images, the rotation $\Delta\widehat{\theta_b}(t)$ that should be caused by the belts by the next frame is computed by

$$\Delta\widehat{\theta_b}(t) = \Delta\widehat{\theta}(t) - (\Delta\theta(t) - \Delta\theta_b(t)), \quad (10)$$

where $\Delta\widehat{\theta}(t)$ is calculated by (2).

TABLE 1. The specifications of the hand, the devices, and the parts.

Maximum width of fingers	60 mm
Material of the belt	Chloroprene rubber(Shore A45)
Thickness of the belt	1 mm
Length of the belt in direction Y	57 mm
Width of the belt in direction Z	30 mm
Motor	Dynamixel XL330-M288-T
Camera	RealSense D405 (Intel)
Resolution	848x480 pixel
Camera-hand distance	70 mm

TABLE 2. The software setups of the process.

K_θ / $K_{f,pos}$ / $K_{b,pos}$	0.3 / 0.5 / 0.1
X_{goal} / Y_{goal} / θ_{goal}	0.0 mm / −41.0 mm / 360.0°
δ_w	4.7 mm

Finally, the required displacement of the left and right belts $\Delta\widehat{b_l}(t)$ and $\Delta\widehat{b_r}(t)$ by the next frame is defined by the following equations:

$$\begin{pmatrix}\Delta\widehat{b_l}(t)\\ \Delta\widehat{b_r}(t)\end{pmatrix} = K_{b,pos}\left(Y_{goal} - C^Y_{pos}(t+1|t)\right)\begin{pmatrix}1\\1\end{pmatrix} + \begin{pmatrix}R(t)\Delta\widehat{\theta_{b,l}}(t)\\ -R(t)\Delta\widehat{\theta_{b,r}}(t)\end{pmatrix}. \quad (11)$$

Here $K_{b,pos}$ is the translation gain, and $\Delta\widehat{\theta_{b,l}}(t)$ and $\Delta\widehat{\theta_{b,r}}(t)$ are the results of (10) for the left and right sides, respectively.

As well as the finger commands, the control commands for the belts, $\hat{b}_l(t)$ and $\hat{b}_r(t)$, are given by dividing $\Delta\widehat{b_l}(t)$ and $\Delta\widehat{b_r}(t)$ by the time Δt.

VI. EXPERIMENT ON OBJECTS WITH VARIOUS SHAPES

The effectiveness of the proposed system has been verified through in-hand manipulation experiments to translate and rotate various types of objects. Please refer to the supplemental videos for the manipulation experiments.

A. EXPERIMENTAL SETUP

1) HAND CONSTRUCTION

The robotic hand shown in Section IV-A was used. Additional design specifications are detailed in Table 1. The experimental setup is described in Fig. 11. The robotic hand was mounted on the fixed base. A stereo camera was attached to the hand via a bracket and arranged so that the hand workspace directly in front of it can be captured.

2) PARAMETERS AND GOALS

The software setups for implementing the system are detailed in Table 2. Specifically, the goal angle of 360°, i.e., 1 revolution, was given because one purpose of the system is to achieve a large range of rotation.

3) DETAILS OF THE TESTED SAMPLES

One purpose of the proposed method is to enable various types of objects to be manipulated. In the experiments,

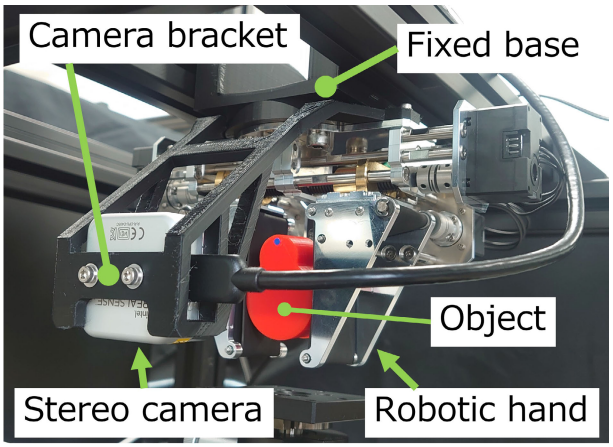

FIGURE 11. The experimental setup. The robotic hand is mounted to the fixed base. A stereo camera is attached to the hand via a camera bracket.

TABLE 3. The cross-sectional shapes and rotatable angles of the objects used in the related works. In the first column, the variety of the shapes are shown. The maximum angle through which rotation was possible for each object is described in the second column. The works using each shape is listed in the third column.

Shape	Angle (max.)	Work
Circle	360°	[8]–[11], [18]–[20] [27]–[29], [31], [32]
Square	360°	[8], [10], [11], [15]–[17] [19], [20], [24]–[26], [28]
Rectangle (4:3)	90°	[20], [25]
Rectangle (3:2)	90°	[8], [9], [32]
Triangle	20.7°	[10]
Ellipse (10:7)	Unknown	[9]
Pear	55.7°	[8], [9]

32 samples consisting of 16 shapes and 2 sizes were tested. In Fig. 12, the variety of the shapes for the large ones is represented with the size values of the cross section. The small ones were prepared as homothetic shapes whose dimensions, indicated by the blue arrows, were 22.5 mm. All samples had the same thickness, 20 mm in direction Z. All samples were produced by a 3D printer with polylactic acid (PLA) plastic. A blue marker was placed on the observable surface to calculate the orientation θ of each object. The angle between the X axis and the line connecting the object centroid $c_{pos}(t)$ and the marker was defined as the orientation $\theta(t)$ at the time t.

In the selection of the shapes to validate the grasping capability, we referred to the objects manipulated in the related works listed in Table 3. In the table, the cross-sectional shapes of the objects and the maximum rotatable angle of each are represented. Also, the works in which each shape was used are cited in the table. For Rectangle and Ellipse, the aspect ratios are also noted, e.g. Rectangle (4:3) means a rectangular cross-section shape which has 4 to 3 aspect ratio. Note that, for the works in which the rotatable angles were not detailed, they are just cited or "Unknown" is written in the column of "Angle (max.)". In the experiments, far more shapes than those were selected, considering the number of vertices, aspect ratio, symmetry, and convexity of each.

TABLE 4. Details of the testing conditions. Each row indicates whether each control was used.

Condition	Method		
	Proposed	A	B
Prediction of contact points (Section V-B and V-C)	True	True	False
Belt deflection and calculation of rotation (Section V-D and V-E)	True	False	False

B. EVALUATION AND COMPARISON

10 trials per sample were conducted. For evaluation, both the average rotation angle for each sample and the ratio of successfully completed trials were calculated.

In addition to the proposed method, other two methods were executed to demonstrate the validity of the proposed one by comparing it with multiple systems. Each condition is abstracted in Table 4 and detailed in the following subsections.

1) METHOD A WITH THE PREVIOUS SYSTEM

Method A is the same as the previous method but with the processes explained in Subsection V-B and V-C. The proposed method differs in considering the situations represented in Sub-subsection III-A2 and Subsection III-B: when the object is easy to drop due to the rotation induced by factors other than the belts and the object is difficult to rotate.

The difference in the control command of the finger (calculated by(7)) was the deflection $\delta_{deflect}$. In Method A, $\delta_{deflect}$ was given by $X_m = 1.25$ mm, the same as in the previous work [33]. Moreover, in Method A, the difference between the observed rotation of the object and the rotation caused by the belts is not calculated. Therefore, the desired angle of the object by the next frame is equal to (2), as follows:

$$\begin{pmatrix} \Delta\widehat{\theta_{b,l}}(t) \\ \Delta\widehat{\theta_{b,r}}(t) \end{pmatrix} = \begin{pmatrix} \Delta\widehat{\theta}(t) \\ -\Delta\widehat{\theta}(t) \end{pmatrix}. \tag{12}$$

2) METHOD B WITH NO NOVEL PROCESS

Method B is the one without using our proposed processes. The results of manipulation under this condition represent to the capabilities just using active surfaces (especially belts) alone. Comparing the performance of the proposed method with this baseline is equivalent to comparison with the works in [5], [21], [22], [28], [29], [30], and [31]. The proposed method differs in considering all challenging situations represented in Section III: when the object is easy to drop and is difficult to rotate.

The fingers were controlled to both follow the current contact point and translate the object to the goal position X_{goal} on the X axis. Therefore, the commands for the fingers were

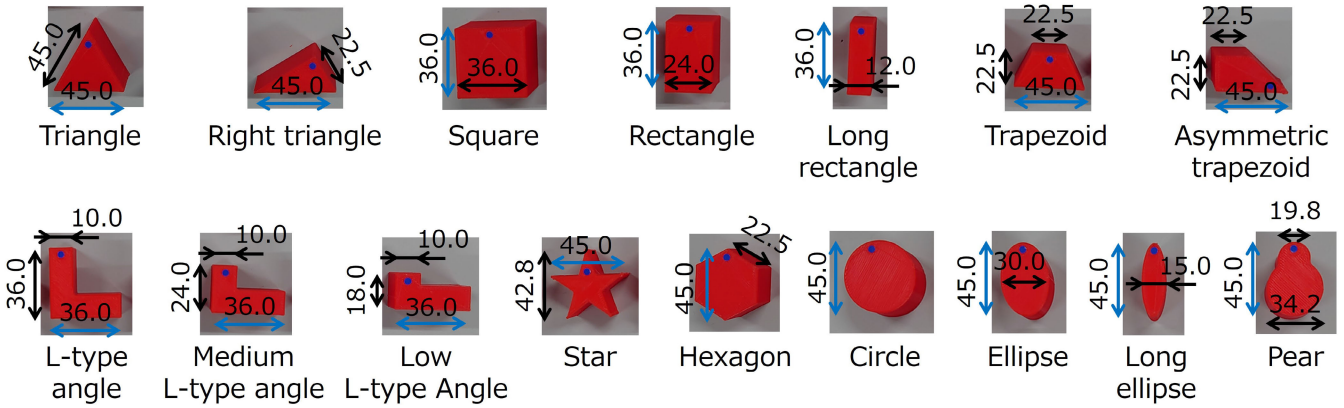

FIGURE 12. The appearance of tested samples with their dimensions (mm). In total, 32 samples, consisting of 16 shapes and 2 sizes (large/small samples of similar shapes), were tested. These are the large ones; the others had homothetic shapes whose dimensions, indicated by the blue arrows, were 22.5 mm. The thickness of all samples was 20 mm in direction Z.

calculated as follows:

$$\begin{pmatrix} \Delta\widehat{f_l}(t) \\ \Delta\widehat{f_r}(t) \end{pmatrix} = K_{f,pos}(X_{goal} - C^X_{pos}(t)) \begin{pmatrix} 1 \\ 1 \end{pmatrix} + \begin{pmatrix} P^X_{cl}(t) - f_l(t) \\ P^X_{cr}(t) - f_r(t) \end{pmatrix} + \begin{pmatrix} X_m \\ -X_m \end{pmatrix}, \quad (13)$$

where the term of the deflection was given by X_m as well as Method A.

The belts were commanded to both rotate the object at the fixed velocity and translate it along the Y axis. In Method B, the control commands for the belts were calculated as follows:

$$\begin{pmatrix} \Delta\widehat{b_l}(t) \\ \Delta\widehat{b_r}(t) \end{pmatrix} = K_{b,pos} \left(Y_{goal} - C^Y_{pos}(t)\right) \begin{pmatrix} 1 \\ 1 \end{pmatrix} + \begin{pmatrix} \Delta\theta_{fixed} \\ -\Delta\theta_{fixed} \end{pmatrix}, \quad (14)$$

where $\Delta\theta_{fixed}$ is the angle of the object within one frame. $\Delta\theta_{fixed}$ was given so that its derivative value $\dot{\theta}_{fixed}$ with time was 3.3 mm/s, which was the average velocity with Method A.

C. RESULTS

The results of the experiments are illustrated in Table 5. Through all trials, the success rate with the proposed method was the highest: 68.8 % for large samples, 75.0 % for small samples, and 71.9 % overall. Meanwhile, the success rates with methods A and B were 50.0 % for large samples, 60.0 % and 55.6 % for small samples, and 55.0 % and 52.8 % overall, respectively. The details of the rotation angle for each sample are shown in Table 6. In the table, the cases in which the goal was achieved are in bold red type. For the cases in which the given goal could not be achieved with any of the methods, the results are in non-bold type; in particular, each maximum angle in all methods is in red type. In the bottom rows of the table (Total), the average results for all shapes are shown as the overall results for each large and small sample. The overall angles with the proposed method were larger than with the other methods, by more than 53.32° for the large ones and 45.25° for the small ones. Moreover, the overall standard deviations with the proposed method were small. Additionally, the variety of the shapes that could be rotated to 1 revolution by the proposed method was wider than that in the other works (See Table 3). The frame rates throughout the experiments were 43.6, 42.4 and 42.6 (fps) for the proposed method, Method A and Method B, respectively. The results and comparisons indicate that both the rotatable angles of the objects and the variety of the manipulatable objects were improved.

TABLE 5. The success rates in achieving the goals. In addition to the success rates, the rates of failure to rotate the samples any more within the hand, and those of dropping them from the hand are shown.

Case	Size	Method		
		Proposed	A	B
Success(%)	large	68.8	50.0	50.0
	small	75.0	60.0	55.6
	total	71.9	55.0	52.8
Failure to rotate(%)	large	5.6	10.0	0.0
	small	25.0	21.3	18.8
	total	15.3	15.6	9.4
Dropping(%)	large	25.6	40.0	50.0
	small	0.0	18.8	25.6
	total	12.8	29.4	37.8

D. DISCUSSION

As a result of the experiments, the goal could be achieved with 23 of 32 samples. By comparing the proposed method with methods A and B, more than 7 samples could be successfully manipulated. As mentioned above, Method B indicates the condition just using active surface alone, which is similar to the related works [5], [21], [22], [28], [29], [30], [31]. Therefore, it can be seen that the proposed control method could achieve higher performance than these works and also our previous method [33], i.e. Method A.

TABLE 6. The results for the rotational angle (°). The results in bold red type are cases in which the goals were achieved. Those in non-bold type are cases in which the objects were dropped during manipulation; the maximum angles of these cases are indicated in red.

Shape	Size	Proposed method		Method A		Method B	
		ave.	std. dev.	ave.	std. dev.	ave.	std. dev.
Triangle	large	**359.29**	0.48	**359.07**	0.06	**360.77**	0.67
	small	**359.81**	0.83	**359.57**	0.80	**359.75**	0.79
Right triangle	large	52.61	2.79	49.83	7.88	51.08	4.62
	small	110.63	5.61	105.85	7.26	101.67	5.06
Square	large	**359.21**	0.35	**359.48**	0.43	**359.48**	0.75
	small	**359.17**	0.12	**359.15**	0.10	**359.13**	0.11
Rectangle	large	**359.25**	0.18	91.51	0.48	78.06	1.37
	small	**359.16**	0.16	90.40	1.24	90.16	1.44
Long rectangle	large	64.46	1.64	63.83	1.23	63.03	1.86
	small	88.40	1.15	59.49	1.51	58.13	0.84
Trapezoid	large	**359.16**	0.19	84.17	6.02	77.03	1.31
	small	**359.31**	0.16	88.76	1.63	87.52	2.83
Asymmetric trapezoid	large	71.78	1.51	76.00	1.36	74.21	1.51
	small	**360.68**	0.28	293.78	110.77	77.32	2.16
L-type angle	large	**360.66**	0.71	**359.43**	0.30	357.38	3.02
	small	**359.96**	1.18	**359.73**	0.89	**359.55**	0.79
Medium L-type angle	large	**360.11**	0.74	95.37	54.63	76.63	1.54
	small	**360.32**	0.64	348.66	33.96	341.15	56.57
Low L-type angle	large	102.45	10.74	70.30	1.48	69.00	2.72
	small	104.41	4.72	77.41	16.66	70.77	12.54
Star	large	**360.65**	0.83	**359.29**	0.24	**359.42**	0.89
	small	**360.28**	0.64	**359.27**	1.13	**359.40**	0.22
Hexagon	large	**359.12**	0.08	**359.57**	0.35	**359.08**	0.06
	small	**360.71**	1.19	**360.21**	0.90	**360.9**	1.04
Circle	large	**360.81**	0.17	**359.86**	0.75	**359.74**	0.87
	small	**361.11**	0.85	**360.63**	0.99	**361.18**	0.13
Ellipse	large	**360.59**	1.09	**359.34**	0.26	**359.30**	0.60
	small	**359.80**	1.02	**359.51**	0.26	**359.88**	0.87
Long ellipse	large	63.19	1.94	53.86	1.52	51.21	1.69
	small	92.49	2.92	49.34	2.94	47.83	2.54
Pear	large	**359.85**	1.13	**359.16**	1.57	**359.11**	0.06
	small	**359.51**	0.81	**359.99**	0.95	**360.86**	0.81
Total	large	269.57	1.54	216.25	4.91	213.41	1.47
	small	294.73	1.39	249.48	11.38	234.65	5.55

Especially, using the proposed method, no small samples were dropped from the hand workspace, even though some could not be rotated to the goal. The drop rate for the small samples was 18.8 % lower than that with Method A and 25.6 % lower than that with Method B. It is considered that enveloping the object within the hand could contribute to the results with the proposed method when the object was likely to fall. Fig. 13 shows an example of when the object (small Long rectangle) was avoided to be dropped by being enveloped by the belts. In Fig. 13, the time run is from left to right. Before the image in Fig. 13(a) was captured, the object had been rotated gradually counterclockwise. Then, in Fig. 13(b), the object could not remain in its orientation and was shifting away from the belt surface. This situation may be caused because factors other than the belts contributed to the rotation of the object in a counterclockwise direction. Though the orientation of the object changed, the fingers could have already followed the width required not to drop it (Fig. 13(c)), because the deflection was large. Consequently, the object could be kept within the hand workspace. In other words, the object could be enveloped.

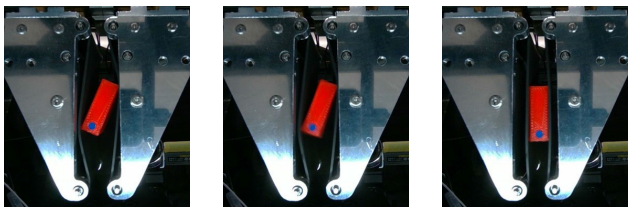

(a) The object was rotated gradually counterclockwise.

(b) The object could not keep its orientation and was shifting away from the belt surface.

(c) The object could remain within the hand.

FIGURE 13. An example of preventing dropping of the object (small Long rectangle). The timeline of the captured images is from the left to right (from (a) to (c)).

However, large samples like the long ellipse could not be enveloped and were dropped from the hand. In order to deal with such issues, inducing a larger belt deflection could be considered, like the configuration in [31]. Another valid option would be to design the surface of the belt with convex and concave geometries [11], as shown in the center image in Fig. 3. This design allows the vertex of the object to remain in the concave part without dropping.

Designing the geometry of the belts is also considered to help solve the problem of failure to rotate the object within the hand. This failure is caused when the appropriate rotation by the belts cannot occur. In the experiments, though increasing

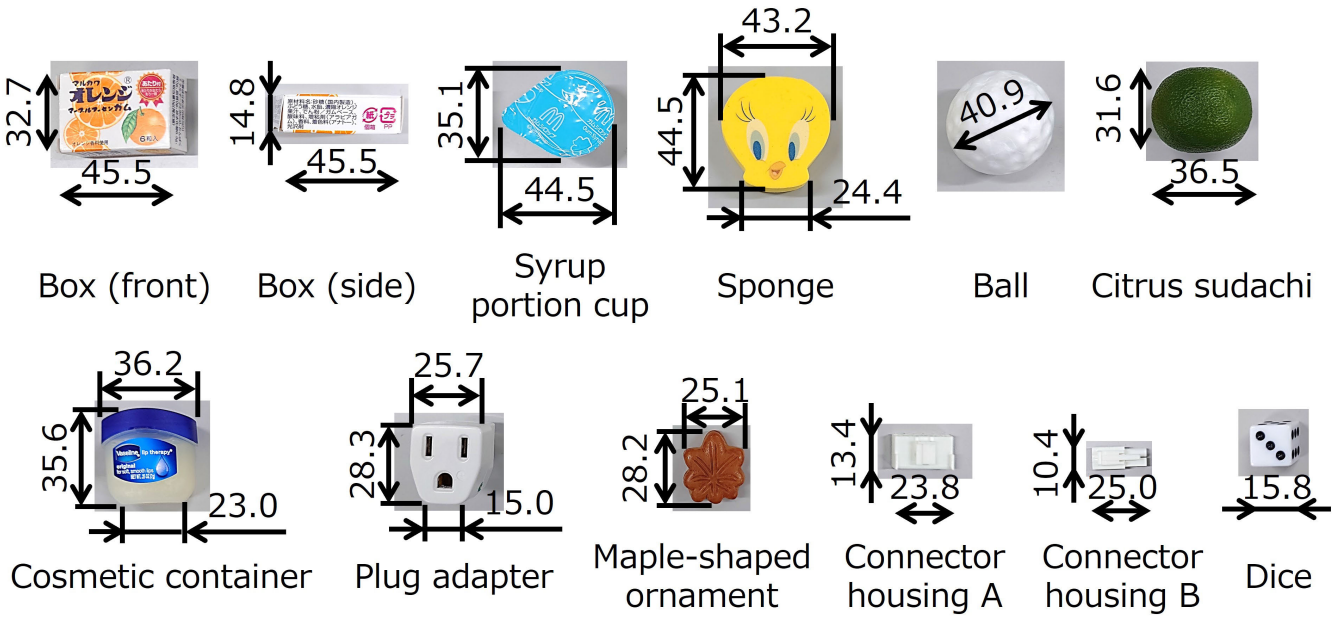

FIGURE 14. The details of the real-world items we tested. The representative dimensions (mm) are shown.

TABLE 7. The results of the experiments for real-world items. The ratio of each case on 10 trials are shown for the respective 12 objects.

Items	Ratio of case (%)		
	Success	Failure to rotate	Dropping
Box (front)	**100.0**	0.0	0.0
Box (side)	0.0	0.0	**100.0**
Syrup portion cup	**100.0**	0.0	0.0
Sponge	**100.0**	0.0	0.0
Ball	**100.0**	0.0	0.0
Citrus sudachi	**100.0**	0.0	0.0
Cosmetic container	**100.0**	0.0	0.0
Plug adapter	**100.0**	0.0	0.0
Maple-shaped ornament	**100.0**	0.0	0.0
Connector housing A	**100.0**	0.0	0.0
Connector housing B	0.0	**100.0**	0.0
Dice	**100.0**	0.0	0.0

the deflection could result in the rotation of some samples (like the rectangle and trapezoid), others, such as the right triangle, still could not be rotated largely. The design of the belt surface may allow the appropriate rotation to occur.

VII. EXPERIMENT ON REAL-WORLD OBJECTS

By using the proposed method, in-hand manipulation has been conducted for real-world objects. The results can also be seen in the supplemental video.

A. EXPERIMENTAL SETUP

The hand construction, the parameters and the goal position (X_{goal} and Y_{goal}) were also same as Sub-section VI-A. The marker to calculate the orientation of the object was not attached to each real object. Instead, each trial was continued until it was visually confirmed whether it was rotated well beyond one revolution or the manipulation was failed (dropped or unable to rotate anymore). Note that, even when the goal orientation is not specified, the system can work till forced termination by fixing $\Delta\theta_{goal}(t)$ in (2) to large value, e.g. 360° as in the experiments.

The 12 real object tested is shown in Fig. 14. These objects were selected by referring the other works in which the real items were manipulated as follows. Box (front / side) and Dice were used by following [20] and [32] and [19], [20], [24], [28], respectively. Ball and Citrus sudachi were prepared as the objects with the sphere and ellipsoid shapes [7], [28], [32]. As the objects with the rounded-corners tested in [20], Cosmetic container and Plug adapter were introduced. Furthermore, the other objects were adopted as the complex shapes with uneven surfaces or varying curvature. To select all items, we also followed same criterion as Sub-subsection VI-A3, and also considered the use cases in manufacturing, logistics, retail and daily life. Note that, the color information used when the contour of the object was extracted in the first process (See Sub-section V-B and Fig. 8(b)) was adjusted for each object. For each item, 10 trials were implemented and the success rate through the trials was calculated as the experimental result.

B. EXPERIMENTAL RESULTS

The results of the experiments is described in Table 7 as the success rate of the manipulation for each item. 10 of the 12 objects could have been manipulated over one revolution with 100% success rates. On the other hand, 2 of them could not achieve the goal even once through all trials. Box (side) were dropped form the hand during manipulation

and Connector housing B could not be rotated more than approximately 90°. The frame rate was 36.7 (fps) throughout the experiments. We also provide the supplemental video showing the manipulation for all objects.

C. DISCUSSION

The experimental results indicated the validity of the proposed method for not only the various objects we designed but also real-world items. Especially, the surfaces of 5 items (Syrup portion cup, Ball, Citrus sudachi, Cosmetic container, Connector housing A) were uneven or curved along the Z direction. The reason that these objects were not dropped is considered because the softness of the belts allowed the belts to follow their surfaces.

However, as in the experiments in Section VI, some objects with high-aspect ratio could not be manipulated as targeted. The aspect ratio of Box (side) was similar to that of Long rectangle in Fig. 12, (3:1). Furthermore, the size of Box (side) was larger than large Long rectangle. As with the results of large Long rectangle, Box (side) was dropped on all trials. Meanwhile, Connector housing B was slightly larger in both aspect ratio and size than those of small Long rectangle. Similar to the results of small Long rectangle, Connector housing B were unable to rotate but were not dropped. Since the results were similar to that of the experiments in Section VI, these failures are thought to be overcome by designing the surface geometry of the belts described in Sub-section VI-D.

VIII. CONCLUSION AND FUTURE WORKS

In this paper, we proposed an in-hand manipulation method for robotic fingers with active surfaces. The purpose of the method was to address the challenge of manipulating a wide variety of objects through a large range of manipulation (especially rotation), with active surfaces. We used a two-fingered parallel gripper with belts made of soft rubber. By using a stereo camera attached to the hand, the shape, orientation and the changes in the contact points of the grasped object were detected. Based on the detection, the belts were controlled to adjust the rotation of the object so that the fingers could follow the object and generate the appropriate rotation. The fingers were controlled to move to the predicted contact points and deflect the belts so as to cancel the unwanted rotation caused by factors other than the belts and produce the desired rotation. Experiments in which 32 objects (16 shapes and 2 sizes) were manipulated to 1 revolution (360°) were conducted and resulted in a higher success rate of 71.9 % as compared to our previous method and other baseline methods. It can be concluded that the proposed system can be used to stably achieve in-hand manipulation with large rotation angles for objects of various shapes and sizes. Additionally, by manipulating the real-world objects, we found that 10 out of 12 objects could be rotated through a complete revolution. The variety of manipulatable objects and the range of manipulation were both wider than in previous studies. We concluded that the proposed method could advance both the grasping and manipulation capabilities, as targeted.

In future works, we will consider the design of the belt so that both the grasping and manipulation capabilities can be enhanced. Especially, we will design the surface geometry of the belts, e.g. convex and concave geometries. The aim is for the object to be enveloped and not to fall from the hand workspace, while the appropriate rotation occurs with a larger range of motion.

REFERENCES

[1] R. R. Ma and A. M. Dollar, "On dexterity and dexterous manipulation," in *Proc. 15th Int. Conf. Adv. Robot. (ICAR)*, Jun. 2011, pp. 1–7.
[2] I. M. Bullock, R. R. Ma, and A. M. Dollar, "A hand centric classification of human and robot dexterous manipulation," *IEEE Trans. Haptics*, vol. 6, no. 2, pp. 129–144, Apr./Jun. 2013.
[3] A. Bicchi, "Hands for dexterous manipulation and robust grasping: A difficult road toward simplicity," *IEEE Trans. Robot. Autom.*, vol. 16, no. 6, pp. 652–662, Dec. 2000.
[4] A. M. Okamura, N. Smaby, and M. R. Cutkosky, "An overview of dexterous manipulation," in *Proc. ICRA Millennium Conf. IEEE Int. Conf. Robot. Autom. Symposia*, Apr. 2000, pp. 255–262.
[5] V. Tincani, M. G. Catalano, E. Farnioli, M. Garabini, G. Grioli, G. Fantoni, and A. Bicchi, "Velvet fingers: A dexterous gripper with active surfaces," in *Proc. IEEE/RSJ Int. Conf. Intell. Robots Syst.*, Oct. 2012, pp. 1257–1263.
[6] N. Chavan-Dafie, K. Lee, and A. Rodriguez, "Pneumatic shape-shifting fingers to reorient and grasp," in *Proc. IEEE 14th Int. Conf. Autom. Sci. Eng. (CASE)*, Aug. 2018, pp. 988–993.
[7] J. Amend and H. Lipson, "The JamHand: Dexterous manipulation with minimal actuation," *Soft Robot.*, vol. 4, no. 1, pp. 70–80, Mar. 2017.
[8] R. R. Ma, W. G. Bircher, and A. M. Dollar, "Toward robust, whole-hand caging manipulation with underactuated hands," in *Proc. IEEE Int. Conf. Robot. Autom. (ICRA)*, May 2017, pp. 1336–1342.
[9] A. S. Morgan, W. G. Bircher, and A. M. Dollar, "Towards generalized manipulation learning through grasp mechanics-based features and self-supervision," *IEEE Trans. Robot.*, vol. 37, no. 5, pp. 1553–1569, Oct. 2021.
[10] Q. Lu, Z. Gan, X. Wang, G. Bai, Z. Zhang, and N. Rojas, "Mechanical intelligence for prehensile in-hand manipulation of spatial trajectories," in *Proc. IEEE Int. Conf. Robot. Autom. (ICRA)*, May 2023, pp. 8075–8081.
[11] A. J. Spiers, B. Calli, and A. M. Dollar, "Variable-friction finger surfaces to enable within-hand manipulation via gripping and sliding," *IEEE Robot. Autom. Lett.*, vol. 3, no. 4, pp. 4116–4123, Oct. 2018.
[12] N. C. Dafle, A. Rodriguez, R. Paolini, B. Tang, S. S. Srinivasa, M. Erdmann, M. T. Mason, I. Lundberg, H. Staab, and T. Fuhlbrigge, "Extrinsic dexterity: In-hand manipulation with external forces," in *Proc. IEEE Int. Conf. Robot. Autom. (ICRA)*, May 2014, pp. 1578–1585.
[13] Y. Hou, Z. Jia, and M. T. Mason, "Fast planning for 3D any-pose-reorienting using pivoting," in *Proc. IEEE Int. Conf. Robot. Autom. (ICRA)*, May 2018, pp. 1631–1638.
[14] N. Chavan-Dafle and A. Rodriguez, "Stable prehensile pushing: In-hand manipulation with alternating sticking contacts," in *Proc. IEEE Int. Conf. Robot. Autom. (ICRA)*, May 2018, pp. 254–261.
[15] A. S. Morgan, K. Hang, B. Wen, K. Bekris, and A. M. Dollar, "Complex in-hand manipulation via compliance-enabled finger gaiting and multi-modal planning," *IEEE Robot. Autom. Lett.*, vol. 7, no. 2, pp. 4821–4828, Apr. 2022.
[16] M. Andrychowicz, "Learning dexterous in-hand manipulation," *Int. J. Robot. Res.*, vol. 39, no. 1, pp. 3–20, 2020.
[17] J. Pitz, L. Röstel, L. Sievers, and B. Bäuml, "Dextrous tactile in-hand manipulation using a modular reinforcement learning architecture," in *Proc. IEEE Int. Conf. Robot. Autom. (ICRA)*, May 2023, pp. 1852–1858.
[18] J. Zhou, J. Yi, X. Chen, Z. Liu, and Z. Wang, "BCL-13: A 13-DOF soft robotic hand for dexterous grasping and in-hand manipulation," *IEEE Robot. Autom. Lett.*, vol. 3, no. 4, pp. 3379–3386, Oct. 2018.
[19] S. Abondance, C. B. Teeple, and R. J. Wood, "A dexterous soft robotic hand for delicate in-hand manipulation," *IEEE Robot. Autom. Lett.*, vol. 5, no. 4, pp. 5502–5509, Oct. 2020.

[20] A. Bhatt, "Surprisingly robust in-hand manipulation: An empirical study," in *Proc. Robot., Sci. Syst.*, 2021, doi: 10.15607/RSS.2021.XVII.089.
[21] K. Morino, S. Kikuchi, S. Chikagawa, M. Izumi, and T. Watanabe, "Sheet-based gripper featuring passive pull-in functionality for bin picking and for picking up thin flexible objects," *IEEE Robot. Autom. Lett.*, vol. 5, no. 2, pp. 2007–2014, Apr. 2020.
[22] T. Nishimura and T. Watanabe, "Single-motor robotic gripper with three functional modes for grasping in confined spaces," *IEEE Robot. Autom. Lett.*, vol. 8, no. 11, pp. 7408–7415, Nov. 2023, doi: 10.1109/lRA.2023.3315559.
[23] A. Kakogawa, H. Nishimura, and S. Ma, "Underactuated modular finger with pull-in mechanism for a robotic gripper," in *Proc. IEEE Int. Conf. Robot. Biomimetics (ROBIO)*, Dec. 2016, pp. 556–561.
[24] S. Yuan, A. D. Epps, J. B. Nowak, and J. K. Salisbury, "Design of a roller-based dexterous hand for object grasping and within-hand manipulation," in *Proc. IEEE Int. Conf. Robot. Autom. (ICRA)*, May 2020, pp. 8870–8876.
[25] S. Yuan, L. Shao, C. L. Yako, A. Gruebele, and J. K. Salisbury, "Design and control of roller grasper v2 for in-hand manipulation," in *Proc. IEEE/RSJ Int. Conf. Intell. Robots Syst. (IROS)*, Oct. 2020, pp. 9151–9158.
[26] K. Tahara, K. Maruta, and M. Yamamoto, "External sensorless dynamic object manipulation by a dual soft-fingered robotic hand with torsional fingertip motion," in *Proc. IEEE Int. Conf. Robot. Autom.*, May 2010, pp. 4309–4314.
[27] J. M. Gómez-de-Gabriel and H. A. Wurdemann, "Adaptive underactuated finger with active rolling surface," *IEEE Robot. Autom. Lett.*, vol. 6, no. 4, pp. 8253–8260, Oct. 2021.
[28] V. Tincani, G. Grioli, M. G. Catalano, M. Garabini, S. Grechi, G. Fantoni, and A. Bicchi, "Implementation and control of the velvet fingers: A dexterous gripper with active surfaces," in *Proc. IEEE Int. Conf. Robot. Autom.*, May 2013, pp. 2744–2750.
[29] R. R. Ma and A. M. Dollar, "In-hand manipulation primitives for a minimal, underactuated gripper with active surfaces," in *Proc. 40th Mech. Robot. Conf.*, vol. 5A, Aug. 2016, pp. 1–7.
[30] T. Ko, "A tendon-driven robot gripper with passively switchable underactuated surface and its physics simulation based parameter optimization," *IEEE Robot. Autom. Lett.*, vol. 5, no. 4, pp. 5002–5009, Oct. 2020.
[31] N. Govindan and A. Thondiyath, "Design and analysis of a multimodal grasper having shape conformity and within-hand manipulation with adjustable contact forces," *J. Mech. Robot.*, vol. 11, no. 5, Oct. 2019, Art. no. 051012.
[32] Y. Cai and S. Yuan, "In-hand manipulation in power grasp: Design of an adaptive robot hand with active surfaces," in *Proc. IEEE Int. Conf. Robot. Autom. (ICRA)*, May 2023, pp. 10296–10302.
[33] Y. Isobe, "Vision-based in-hand manipulation of variously shaped objects via contact point prediction," in *Proc. IEEE Int. Conf. Intell. Robots Syst.*, Oct. 2023.
[34] D. H. Douglas and T. K. Peucker, "Algorithms for the reduction of the number of points required to represent a digitized line or its caricature," *Cartographica, Int. J. Geographic Inf. Geovisualization*, vol. 10, no. 2, pp. 112–122, Dec. 1973.
[35] C. B. Barber, D. P. Dobkin, and H. Huhdanpaa, "The quickhull algorithm for convex hulls," *ACM Trans. Math. Softw.*, vol. 22, no. 4, pp. 469–483, Dec. 1996.

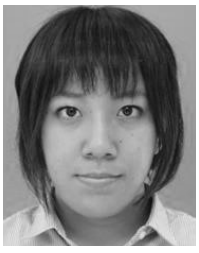

YUZUKA ISOBE received the B.Eng. and M.Eng. degrees in mechanical engineering from Chuo University, Japan, in 2016, where she is currently pursuing the Ph.D. degree in precision engineering.

In 2016, she joined Panasonic Corporation and transferred to Panasonic Connect Company Ltd., in 2022, where she has been with since then. Her research interests include the development of robot vision and robot control systems.

SUNHWI KANG received the B.S., M.S., and Ph.D. degrees in engineering from Osaka University, Osaka, Japan, in 2017, 2019, and 2022, respectively.

He has been with Panasonic Connect Company Ltd., since 2022. His research interests include the development of identification and a control method for robots using dynamical model-based control theories.

TAKESHI SHIMAMOTO received the M.Eng. degree in robotics (major) from Ritsumeikan University, Japan, in 2002.

He joined Matsushita Electric Industrial Company Ltd. (currently Panasonic Holdings Company Ltd.), in 2002, and transferred to Panasonic Connect Company Ltd., in 2022, where he has been with since then.

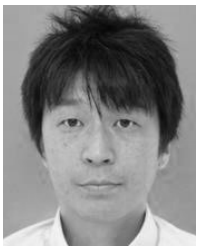

YOSHINARI MATSUYAMA received the M.Eng. degree in robotics (major) from Ritsumeikan University, Japan, in 2008.

He is currently with Panasonic Connect Company Ltd., on the development of a robot control systems.

SARTHAK PATHAK (Member, IEEE) received the B.T. and M.T. dual degree from the Department of Engineering Design, Indian Institute of Technology Madras, India, in 2014, and the Ph.D. degree from the Department of Precision Engineering, The University of Tokyo, Japan, in 2017.

He was a Postdoctoral Researcher and a Project Assistant Professor with The University of Tokyo. Following that, he moved to the Chuo University, Tokyo, Japan, as an Assistant Professor of precision mechanics. His main research interests include robot vision, specifically, localization, 3-D reconstruction, and SLAM, especially using 360-degree cameras.

KAZUNORI UMEDA (Member, IEEE) received the B.Eng., M.Eng., and Ph.D. degrees in precision machinery engineering from The University of Tokyo, Japan, in 1989, 1991, and 1994, respectively.

He became a Lecturer of precision mechanics with Chuo University, Japan, in 1994, and has been a Professor, since 2006. He was a Visiting Worker with the National Research Council of Canada, from 2003 to 2004. His research interests include range image processing, robot vision, and human–machine interface using vision.